JGR

RESEARCH ARTICLE

Correspondence to:
M. Guala,
mguala@umn.edu

Spectral description of migrating bed forms and sediment transport

Michele Guala[1], Arvind Singh[1], Nicholas BadHeartBull[1], and Efi Foufoula-Georgiou[1]

[1]Department of Civil Engineering, St. Anthony Falls Laboratory, National Center for Earth-Surface Dynamics, University of Minnesota, Twin Cities, Minneapolis, Minnesota, USA

Abstract This paper considers the problem of spatiotemporal bed topography evolution and sediment transport estimation in rivers with migrating bed forms of different types and sizes, in statistical equilibrium conditions. Instead of resorting to bed form classification, we propose to evaluate the evolution of multiscale bed topography as the integral of unit contributions defined through a space-time Fourier decomposition of bed elevations. Using joint 2-D spectra in the frequency and wave number domain, a functional relationship between the length scales and the timescales in which migrating bed forms are decomposed is proposed and developed into a dimensionless expression for scale-dependent convection velocities. This formulation highlights the violation of Taylor's hypothesis for migrating bed forms, confirming statistically that larger bed forms travel slower as compared to smaller bed forms. This phenomenological description leads to a spectral extension of the Simons et al. (1965) formula for sediment transport to incorporate a range of multiscale migrating features. Both the scaling of convection velocities and the spectral estimate of sediment transport rate were validated through extensive bed elevation data from laboratory experiments conducted at the St. Anthony Falls Laboratory, for a range of Froude numbers $0.2 < Fr < 0.5$, under varying discharge and bed material composition.

1. Introduction

Estimating sediment transport rate in the presence of bed forms has been challenging researchers for many decades since the early work of *Bagnold* [1946]. The wide range of bed form types and geometries, as well as their dynamic interactions, has always been a challenge to a generalized statistical approach to estimating sediment transport under varying discharge and grain size distributions. Large-scale bed forms such as alternate bars, for instance, obey specific scaling relationships and mechanisms of instability, as emphasized by a number of studies [*Ikeda*, 1984; *Colombini et al.*, 1987; *Seminara*, 2010, and references therein]. These are different from those of dunes [*Engelund and Fredsoe*, 1982; *Kennedy*, 1963; *Best*, 2005; *Venditti et al.*, 2005a; *Coleman et al.*, 2006; *Colombini and Stocchino*, 2011], ripples, chevrons, or antidunes [*Stegner and Wesfreid*, 1999; *Betat et al.*, 1999; *Fourriere et al.*, 2010; *Andreotti et al.*, 2012]. Some of these contributions employed linear stability analysis to explore how different bed form types result from the amplification of specific initial perturbations starting from flatbed conditions and how, for each bed form type, a key length scale (e.g., scaling with the channel width or depth) can be derived corresponding to the most unstable perturbation. These theoretical predictions have been validated by laboratory experiments reporting the dominant bed form wavelength and height [*Guy et al.*, 1966; *Jaeggi*, 1984; *Colombini et al.*, 1987, and references therein]. In many realistic conditions, however, different bed form types and sizes were observed to overlap, interact and/or merge into complex migrating bed forms [see, e.g., *Jerolmack and Mohrig*, 2005; *Venditti et al.*, 2005b; *Martin and Jerolmack*, 2013].

In addition, bed forms of the same type can exhibit a significant variability and thus display a wide range of wavelengths and heights [*Hino*, 1968; *Nikora et al.*, 1997; *van der Mark et al.*, 2008; *McElroy and Mohrig*, 2009; *Singh et al.*, 2011, among others]. The statistical variability in bed form shape and size and the possible superimposition of different bed form types suggest that several length and timescales need to be accounted for in capturing the evolution of complex riverbed topography in natural environments [*Allen*, 1968; *Rubin and McCulloch*, 1968]. While studying the initial growth of competing perturbations of different sizes poses several theoretical challenges, the evolution of multiscale bed topography can be addressed rather simply, once bed forms have reached a statistically steady state. We consider herein the case of migrating bed forms in a straight flume in dynamical equilibrium conditions, and we focus on their spatiotemporal evolution and their effect on sediment transport. We specifically explore a framework in which

bed form classification and extraction is not strictly necessary to quantify their contribution to sediment transport. Instead of working in the physical domain to estimate individual bed form heights and lengths, we decompose bed elevation series into a space-time wave number, frequency domain, and integrate over a range of scales to capture the contribution of the multiscale migrating features of complex bed topography to the total sediment transport.

Since the early work of *Simons et al.* [1965] the connection between sediment transport rate and bed form characteristics has been expressed based on a geometric formulation, as

$$q_s = q_0 + \frac{(1-p)V_b H_b}{2} \tag{1}$$

where q_s is the transport rate per unit width, p is the porosity of the bed material, V_b and H_b are the velocity and height of the statistically dominant, or average, bed form, respectively. The factor 2 in the right-hand side of equation (1) comes from the assumption of a triangular bed form shape, and q_0 represents the contribution to bed load transport that does not enter into the propagation of bed forms. Equation (1) can also be derived from the integration of the Exner equation [*Paola and Voller*, 2005] assuming that, in equilibrium condition, bed forms do not deform while migrating; q_0 appears then as an integration constant which is neglected here [see, e.g., *McElroy and Mohrig*, 2009].

Equation (1) requires only estimates of the average values of V_b and H_b which can be provided using any bed form extraction technique able to identify period and wavelength of each bed form [*van der Mark et al.*, 2008; *McElroy and Mohrig*, 2009; *Singh et al.*, 2011]. Nevertheless, the spatial (or temporal) variability in the bed form geometry, e.g., measured by the standard deviation of an ensemble of bed form heights and wavelengths extracted from the bed topography, is not incorporated in the *Simons et al.* [1965] formulation, which accounts only for the average values. In addition, the coexistence of various sizes of topographic features and types of bed forms, e.g., ripples superimposed on dunes, makes the *Simons et al.* [1965] approach too simplistic, as large bed forms are known to travel slower than smaller bed forms [*Hino*, 1968; *Nikora et al.*, 1997; *Coleman and Melville*, 1994; *Giri and Shimizu*, 2006; *Schwämmle and Herrmann*, 2004; *Singh et al.*, 2011]. This induces a second element of dynamic variability which adds to the intrinsic spatial variability of bed forms, resulting in a modulated temporal evolution of the bed topography. Bed form-dependent propagation velocities are therefore needed to include the effects of spatiotemporal bed form variability and evolution and ultimately extend the *Simons et al.* [1965] approach to the case of complex erodible riverbed topographies with multiscale topographic features and migrating bed forms. By treating any migrating surface feature as a combination of Fourier modes, we introduce a generalized approach to calculating propagation velocities avoiding bed form classification. The propagation velocities of different size bed features are statistically described here in terms of spectral convection velocities $C_v = \omega/k$, where k and ω are the wave number and frequency of the different scale Fourier modes in which the evolving topography is decomposed.

Similar ideas have been used in the turbulent boundary layer community where a spectral approach has been pursued to estimate scale-dependent convection velocities to test the applicability of Taylor's hypothesis of frozen turbulence [*Morrison et al.*, 1971; *Erm and Joubert*, 1991; *Krogstad et al.*, 1998; *Dennis and Nickels*, 2008; *Chung and McKeon*, 2010; *LeHew et al.*, 2011, among others]. Essentially, Taylor assumed that turbulent flow structures on average move with the local (i.e., at fixed height) mean velocity, implying that a velocity signal recorded in time can be projected in space via a simple renormalization with no information loss. Testing Taylor's hypothesis requires that the convection velocity of different turbulent structures can be estimated. Since those structures are not easily identifiable in the physical domain, the spectral approach is pursued using velocity measurements simultaneously obtained in time and space. Time-resolved particle image velocimetry measurements were used for this specific purpose in *LeHew et al.* [2011] in the case of a flat plate turbulent boundary layer flow. Scale-dependent convection velocities were then estimated by means of two-dimensional spectra in the frequency and wave number(s) domain. We propose here a similar approach to quantify the scale-dependent velocities of migrating bed forms based on measurements of evolving surface topography $z = z(x, t)$, instead of flow velocity spatiotemporal series $v = v(x, t)$. Note that a quantification of the propagation velocities of bed forms of different scales was performed by *Singh et al.* [2011] using only temporal elevation data and employing a wavelet-based correlation analysis. That study suggested that smaller bed forms move faster than larger ones.
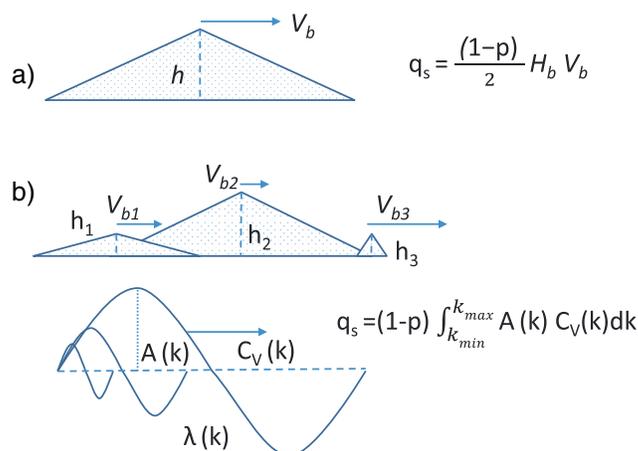
Figure 1. Conceptual model for the estimate of sediment transport rates q_s extending *Simons et al.* [1965] approach (a) to a Fourier-based model (b) accounting for multiscale bed forms with scale-dependent convection velocities and arbitrary shape; ($\lambda(k)$, $C_v(k)$ and $A(k)$ are the wavelength, convection velocity, and amplitude, respectively, of the Fourier mode k in which bed forms are decomposed).

Experimental observations of large bed forms statistically propagating slower than smaller bed forms [*Coleman and Melville*, 1994; *Giri and Shimizu*, 2006; *Schwämmle and Herrmann*, 2004; *Singh et al.*, 2011; *Martin and Jerolmack*, 2013] can be interpreted as the result of smaller bed forms merging into larger ones. This mechanism suggests that (i) the evolution of bed topography is the result of the coupling between bed form advection and deformation processes; therefore, (ii) Taylor's assumption of a single convective velocity is not expected to represent correctly migrating bed forms in nature, and ultimately, (iii) *Simons et al.* [1965] approach may not provide an accurate estimate of sediment transport rate in complex topographic conditions. These observations suggest the possibility of extending *Simons et al.* [1965] model to include multiscale bed form migration and deformation processes through the introduction of scale-dependent convection velocities. Such a conceptual framework is shown in Figure 1, where different size bed forms are represented by different sinusoids: note that as the bed form height is conventionally defined from trough-to-crest, the corresponding sinusoid amplitude must be doubled and its specific sediment discharge contribution is proportional to $A(k)C_v(k)$. We stress that multiscale bed forms are intended here to account for the multiscale variability of the evolving bed topography, including as special cases the coexistence of different bed form types as well as the spatiotemporal variability within each bed form type.

The first goal of this paper is to propose a spectral description of evolving surface bed elevations, in both the frequency and wave number domain, and provide a method to estimate scale-dependent convection velocities for migrating topographic features. The second goal is to identify, for the case of migrating bed forms in equilibrium conditions, a scaling relationship between the period and wavelength of the Fourier decomposed bed forms, propose a set of normalizing variables and a dimensionless description of convection velocities. Finally, we pursue a generalization of the *Simons et al.* [1965] approach toward the formulation of a sediment transport rate model that explicitly acknowledges the presence of space-time topographic feature of multiple scale. Measurements of evolving bed elevations, $z = z(x, t)$, were obtained by a partially submerged sonar mounted on a computer-controlled cart, covering the flume's central longitudinal transect of 5 m every 13–20 s (depending on the run), for a total of approximately 20 h. Two different sets of experiments were conducted under varying flow discharges using sand (set 1) and fine gravel (set 2) as bed material, in a range of Froude numbers $0.2 < Fr < 0.5$.

The paper is structured as follows. The experimental setup is described in section 2. Spectral analysis is introduced in section 3.1, while scale-dependent convection velocity and key scaling arguments are discussed in section 3.2. An expression for estimation of sediment transport rate in the presence of bed forms is proposed in section 3.3, whereas an alternative scaling option is discussed in section 4. Finally, concluding remarks are given in section 5.

GUALA ET AL.   125
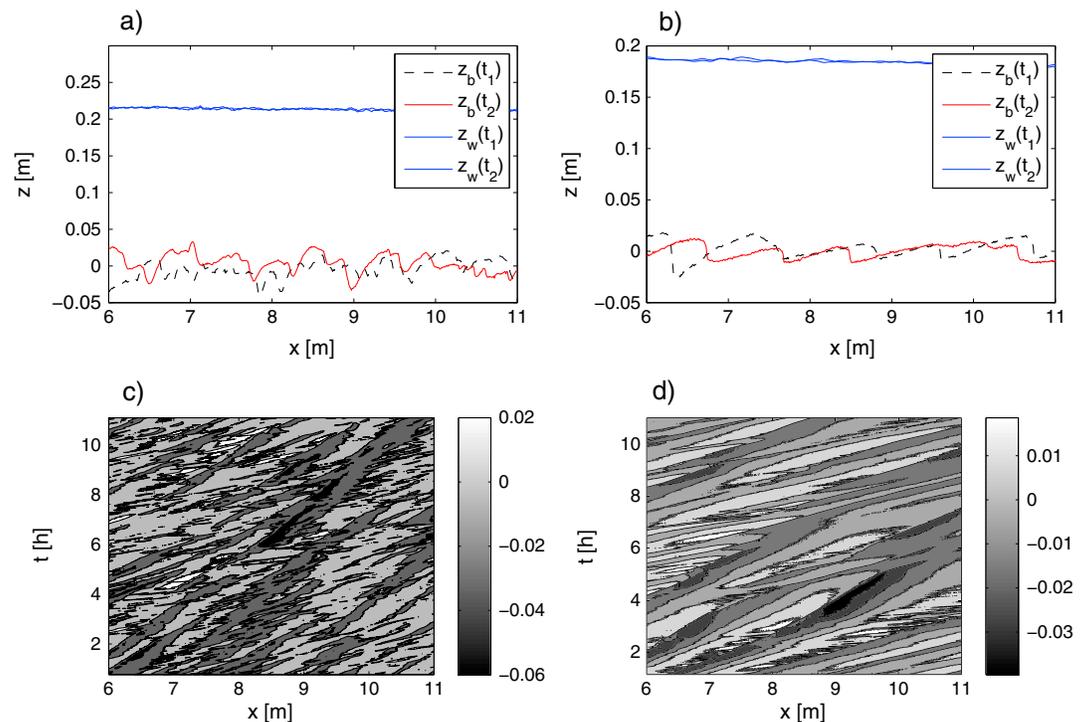
Figure 2. Measurements of bed surface elevation (z_b) and free surface elevation (z_w) along the channel centerline for (a, c) $Q_L = 70$ L s^{-1} and (b, d) $Q_L = 115$ L s^{-1}, corresponding to experiments in Table 1 (columns b and d). Bed surface elevation contours ($z[m]$) in the spatiotemporal domain (x (m), t (h)) are shown in Figure 2c and Figure 2d for the two case studies, respectively.

2. Experimental Setup

Experiments were conducted in the tilting flume of the St. Anthony Falls Laboratory at the University of Minnesota. The flume is 0.9 m wide and 18 m long and is equipped with a sediment recirculation pump system that ensures the rapid establishment of morphodynamic equilibrium conditions: The sediment supply upstream is equal to the transport rate downstream resulting in a rapid stabilization of the mean longitudinal slope. In addition to the bed and water surface slope, bed form characteristics were also monitored in time along the channel centerline, during data acquisition. The standard deviation of bed elevations was computed at different time periods and at different portions of the test section to ensure statistical steady conditions and streamwise homogeneity.

The flume is equipped with a computer controlled cart able to precisely move a set of instruments along the 5 m longitudinal transect. This is the test section that we consider, located between $x = 6$ m to $x = 11$ m, sufficiently far from the inflow ($x = 0$ m) and outflow ($x = 18$ m) conditions. The moving sensors consist of a submerged sonar for bed elevation z_b and a second probe for water surface elevation z_w. Measurements were taken every 0.01 m in the longitudinal direction, and repeated in time. Therefore, our spatial and temporal resolutions are d$x = 10^{-2}$ m and d$t = 13$–20 s, respectively. At a fixed position upstream of the test section, a Vectrino acoustic Doppler velocimeter profiler is used to monitor the inflow conditions and to provide an independent estimate of the Reynolds stresses $\rho < \overline{-u'w'} >$ (where u' and w' are the streamwise and vertical velocity fluctuations, respectively, and ρ is the fluid density). We recall that the shear velocity u_* is a key velocity scale near the surface, controlling both bed form formation and transport rate. By means of a direct measurement u_* can be estimated of velocity fluctuations $u_* = < \overline{-u'w'} >^{1/2}$, or it can be indirectly obtained by the mean momentum equation in uniform flow, $u_* = \sqrt{gRS_w}$, where g is the acceleration due to gravity, R is the hydraulic radius, and S_w is the slope of the water-free surface. The $\sqrt{gRS_w}$ estimator was preferred, as the water surface slope was observed to be extremely steady during the runs. The other scales of interest are the water depth D, obtained by subtracting the bed elevations from the water surface measurements, and the sediment diameter d_s. The two sediment mixtures used in these
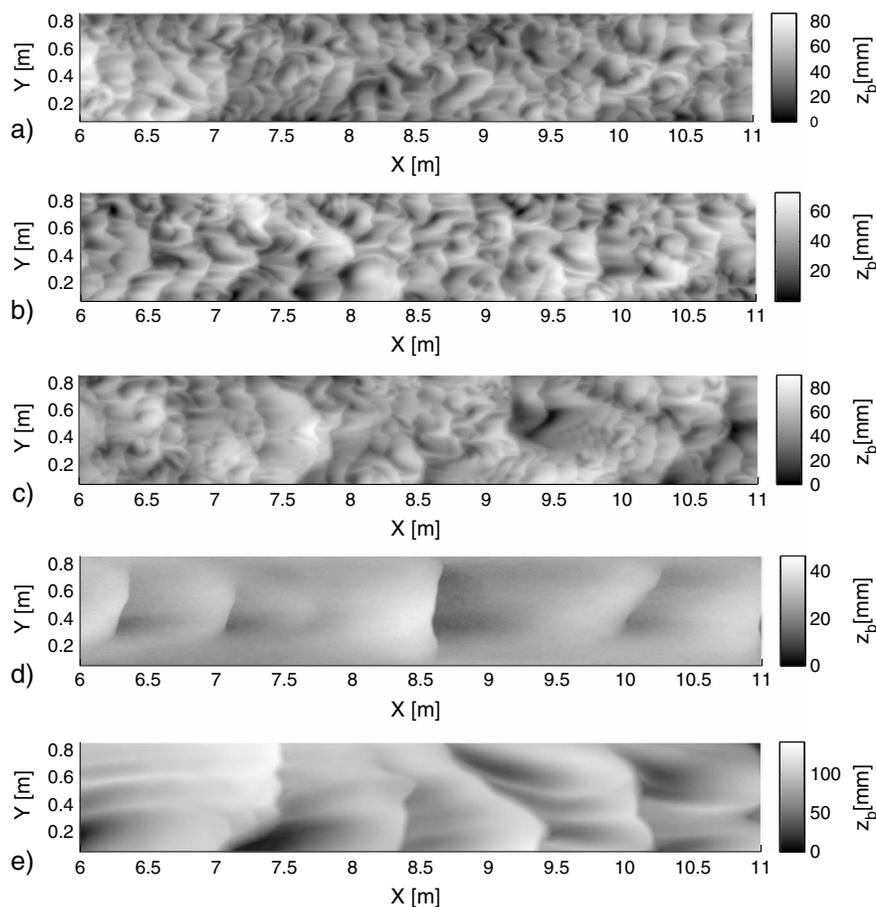
Figure 3. Two-dimensional laser scan of bed topography at the end of the experiment: sand experiments with (a) $Q_L = 60$ L s^{-1}, (b) $Q_L = 70$ L s^{-1}, (c) $Q_L = 80$ L s^{-1}; gravel experiments with (d) $Q_L = 115^{-1}$ and (e) $Q_L = 135^{-1}$ (see Table 1).

experiments have nearly uniform grain size distributions with a median grain size $d_s = 0.0008$ m for the sand experiment and $d_g = 0.0018$ m for the fine gravel experiment, respectively. We acknowledge that sediments with diameter larger than 2 mm are nominally defined as gravel. However, the grain size distribution showed about 35% of the material in the range between 2 mm and 3.5 mm. In order to distinguish the two sets of experiments and recognize the different roughness contributions, this substrate material is referred to as gravel. The flow discharge, estimated through a calibrated triangular weir located at the downstream end of the flume, was varied from 60 to 135 L s^{-1}. Each experiment started with a flat topography and was concluded with a full topographical scan $z = z(x, y)$. An example of the spatiotemporal measurements $z = z(x, t)$ is provided in Figure 2 (contour plot), while results from the full topographical scans are shown in Figure 3. Experimental conditions are summarized in Table 1. Note that bed form characteristics were obtained from an average of 20+ bed forms tracked visually and using the quantitative bed form extraction method of *Singh et al.* [2011] in space and time for each flow discharge. The calculated mean bed form velocities compare well with the lower range values of dune celerities reported by *Simons et al.* [1965] (below 0.1ft/min in their original report).

3. Results

3.1. One-Dimensional Topography Spectra

Bed elevation data $z(x, t)$ were used to compute the surface topography spectra in the wave number and frequency domains [see, e.g., *Nordin and Algert*, 1966; *Hino*, 1968; *Nikora et al.*, 1997; *Aberle et al.*, 2010; *Singh et al.*, 2011]. Spatial Φ_k and temporal Φ_f spectra were computed on linearly detrended longitudinal transects

Table 1. Experimental Conditions and Averaged Bed Form Characteristics

		Sand			Gravel	
Experiments		a	b	c	d	e
Flow discharge Q_L	(L s^{-1})	60	70	80	115	135
Water surface slope S_w		$7.9 \cdot 10^{-4}$	$7.5 \cdot 10^{-4}$	$9.1 \cdot 10^{-4}$	$15 \cdot 10^{-4}$	$19 \cdot 10^{-4}$
Shear velocity u_*	(ms^{-1})	0.038	0.037	0.044	0.053	0.062
Median sediment diameter d_s	(mm)	0.8	0.8	0.8	1.8	1.8
Froude number F		0.26	0.31	0.29	0.48	0.5
Mean bed form height H_b	(m)	0.020	0.024	0.028	0.023	0.04
Mean bed form length $L_{bedform}$	(m)	0.29	0.39	0.48	1.02	1.03
Mean bed form period $T_{bedform}$	(min)	62.9	43.4	45.7	36.1	29.3
Mean propagation velocity V_b	(cm/min)	0.46	0.91	1.06	2.82	3.51

$z(x)$ and time series $z(t)$, respectively, using Fast Fourier Transform (hereafter FFT) and a Hanning window to prevent aliasing. Power spectra were normalized imposing

$$\sigma_x^2(z) = \int_0^{kmax} \Phi_k dk; \quad \sigma_t^2(z) = \int_0^{fmax} \Phi_f df, \quad (2)$$

where $k = 2\pi/\lambda$ is the wave number (λ is the wavelength), f is the frequency, $\sigma_x^2(z)$, and $\sigma_t^2(z)$ are the variance of the bed elevations of the spatial and temporal series, respectively. The maximum (Nyquist) frequency $f_{max} = f_s/2$ is based on the sampling frequency, defined as the inverse of the transect repetition timescale; thus, $f_s = 1/\Delta t$. Similarly, the maximum wave number $k_{max} = \frac{2\pi}{2\Delta x}$ depends on the spatial resolution of the longitudinal scans ($\Delta x = 0.01$ m). The 1-D power spectra of the spatial transects were normalized by the sediment grain size, as shown in Figure 4a. The normalization of the frequency spectra requires, instead, a timescale, which can be obtained by dividing the mean grain diameter by the shear velocity (d_s/u_*) as shown in Figure 4b. As suggested by other studies [e.g., *Hino*, 1968; *Nikora et al.*, 1997; *Singh et al.*, 2011, and references therein] we confirm that the slope of the topography spectra is steeper in the wave number domain as compared to the frequency domain. This can be interpreted as an effect of scale-dependent convection velocities, as discussed in section 3.2. The clear scaling regimes in the spatial and temporal spectra confirm that both the spatiotemporal resolution (Δx, Δt), as well as the transect length and the total duration of the experiment, were sufficient to describe the full range of space-time fluctuations of the bed elevations.

3.2. Two-Dimensional Spatiotemporal Topography Spectra
The 2-D spectra are computed following the procedure described in *LeHew et al.* [2011] applying a 2-D FFT over the full matrix $z = z(x, t)$: the spectra $\Phi_{k,\omega}$ are computed in the wave number (k), and angular frequency
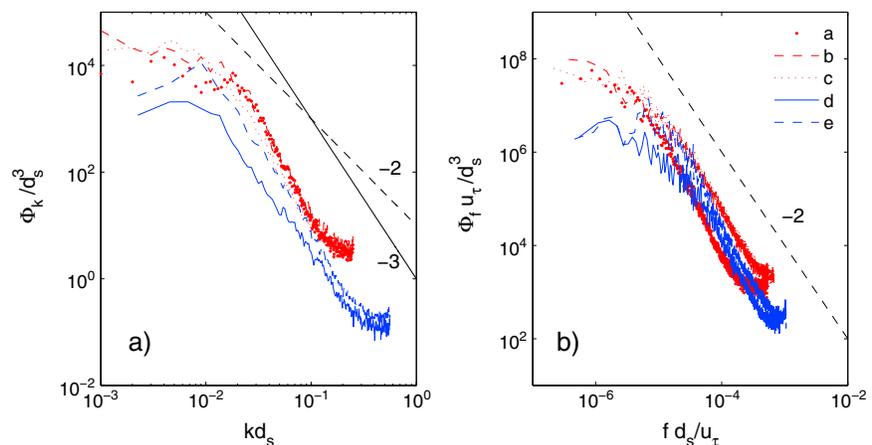
Figure 4. Dimensionless (a) wave number and (b) frequency 1-D spectra: sand experiments are reported in red, while gravel experiments are in blue. The -3 and -2 power scaling parameters (slopes) are plotted for reference.
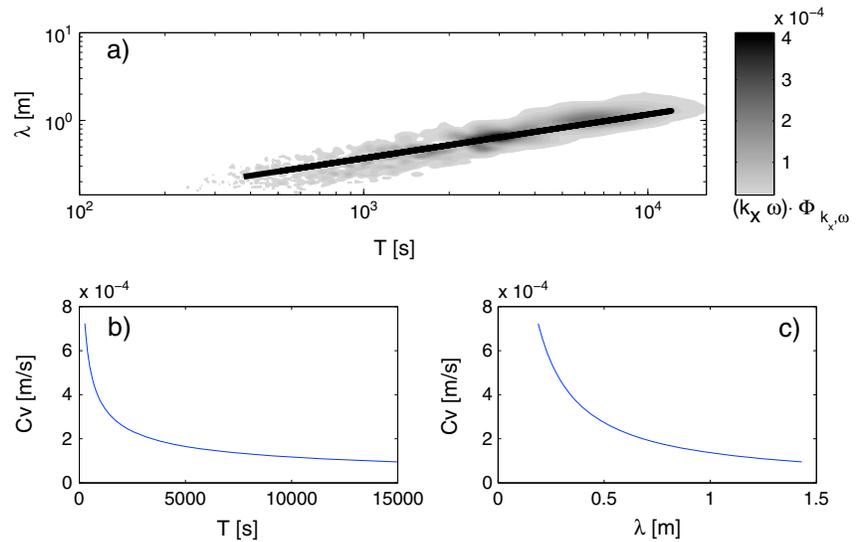
Figure 5. (a) Two-dimensional power spectral density of bed elevation $z(x, t)$ computed in the frequency-wave number domain and plotted as a function of the wave length λ and the period T. Scale-dependent convection velocities C_v are estimated fitting a power law (straight black line) to the ridge of the 2-D power spectrum in the λ, T domain. The obtained trend for the convection velocities is plotted as a function of the (b) period T and (c) wave length λ, respectively. These data are from the sand experiment (Table 1, column c).

domain ($\omega = 2\pi f$). Every point on the ridge of the contour can be identified by a specific wavelength $\lambda = 2\pi/k$ and period $T = 2\pi/\omega$, and thus by a specific (scale-dependent) convection velocity $C_v = \omega/k$ (see Figure 5).

Interestingly, a power law can be used to fit the points on the ridge of the spectra, as shown in Figure 5. The power law defines a functional relationship between λ and T that can be expressed as $\lambda = BT^n$, with the B and n parameters obtained from the fit. It was observed that the exponents n did not vary significantly in the set of experiments analyzed here and could then be assumed to be constant, $n = 1/2$. The dimensional coefficient B however varied significantly among the different experiments, in the range between 0.002 and 0.02 ($ms^{1/2}$). From dimensional analysis we worked out a dimensionless form of this functional relationship based on u_* and d_s, i.e., the two meaningful scales that we identified in the spectral normalization. We propose that the scaling coefficient B can be defined as $B = C\sqrt{u_* d_s}$, with C assumed, for now, constant $C = 2$ (we note that by relaxing the constraint on the constant C, we could infer a weak dependency $C = C(u_*)$ that will be addressed in future investigations in the form of $C = C(Re_*)$ with $Re_* = u_* d_s/\nu$). Combining the above, the functional relationship between λ and T reads

$$\frac{\lambda}{d_s} = C\left(\frac{Tu_*}{d_s}\right)^{1/2}.$$

(3)

We present the spatiotemporal spectra plotted in dimensional variables in Figure 6 and in the dimensionless variables $\frac{\lambda}{d_s}$ and $\frac{Tu_*}{d_s}$ in Figure 7. In contrast to the observed $\lambda \propto T^{1/2}$ relationship, a unique scale-independent convection velocity $C_v = \omega/k = \lambda/T = $ constant in line with Taylor's hypothesis, would imply a $\lambda \propto T$ relationship. The overlap of the different contours in Figure 7 is, to some extent, satisfactory for confirming the representativeness of the chosen scaling quantities and the violation of Taylor's hypothesis. We however acknowledge that the 2-D spectra contour for the lowest discharge case (60 L s^{-1}) does not fit the proposed functional relationship as well as those from the higher discharge experiments. More laboratory or field experiments are needed to confirm the proposed scaling relationship for a wide range of conditions (the exponent n in $\lambda = BT^n$ and the constant C in equation (3) may weakly vary with the discharge and/or bed material compositions).

The functional relationship between wavelength and period revealed by the data indicates that Taylor's hypothesis is not applicable for the case of migrating bed forms, as different scales move with different convection velocities. Specifically, larger scales move slower than smaller scales, possibly as a result of bed forms merging and/or surface deformation processes. Following equation (3), scale-dependent convection
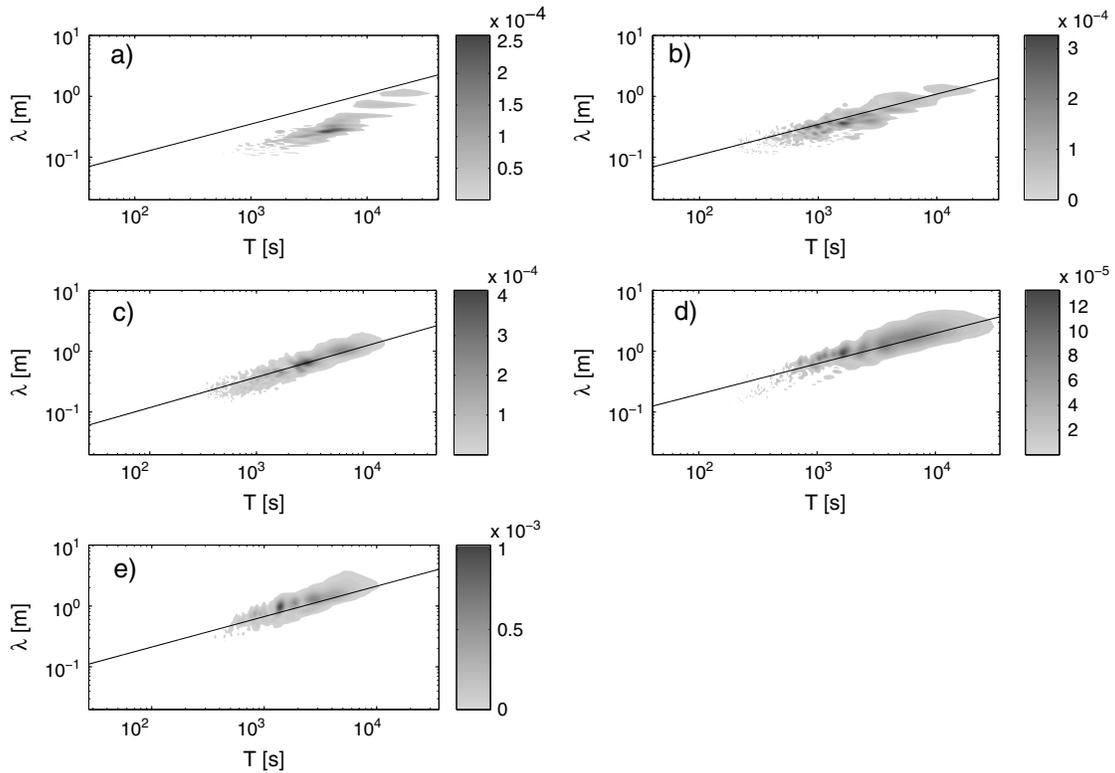
Figure 6. Two-dimensional power spectra $(k \cdot \omega)\Phi_{k,\omega}$ for the five experiments (see Table 1, columns a–e). The solid lines indicate the proposed 1/2 power law dependency $\lambda = C\sqrt{u_* d_s}T^{1/2}$ with $C = 2$.

velocities can be expressed as $C_V(T) = C\sqrt{\frac{u_* d_s}{T}}$ or alternatively $C_V(\lambda) = C^2 \frac{u_* d_s}{\lambda}$. Figures 6 and 7 support the validity of the proposed scaling arguments and the above conclusion. It is noted that the proposed scaling for scale-dependent convection velocities is consistent with the observed steeper slope of the 1-D wave number spectra of bed elevation as compared to the frequency spectra (Figure 4). The formal relationship between frequency and wave number spectra is provided in the following section.

3.3. Frequency to Wave Number 1-D Spectra Transformation

The scaling regime of the bed elevation spectrum in the angular frequency domain $\Phi_\omega(\omega)$ is derived here as a function of the corresponding spectrum in the wave number domain $\Phi_k(k)$ and of the scale-dependent convection velocity. Starting from $\Phi_k(k)dk = \Phi_\omega(\omega)d\omega$ and the scale-dependent velocity $C_V = \omega/k$ we derive:

$$\Phi_\omega(\omega) = \Phi_k(k)\frac{dk}{d\omega} = \frac{\Phi_k(k)}{C_V(k) + k\frac{dC_V(k)}{dk}} \tag{4}$$

Consistent with the observed power law spectra $\Phi_k(k)$ and $\Phi_\omega(\omega)$ within a range of scales, a power law expression for C_V is assumed in the form $C_V(k) \propto k^\beta$, with $\beta > 0$ in agreement with field and laboratory results showing small bed forms (high k) traveling faster (high C_V) than larger bed forms. Then we can express $k = \omega^{\frac{1}{\beta+1}}$, and by substituting $\Phi_k(k) \propto k^{-\alpha}$ we obtain

$$\Phi_\omega(\omega) \propto \frac{k^{-\alpha}}{k^\beta + k\beta k^{\beta-1}} = \frac{1}{1+\beta}\omega^{-\gamma} \qquad \text{where} \qquad \gamma = \frac{\alpha+\beta}{\beta+1} \tag{5}$$

If Taylor's hypothesis holds, in the transformation from frequency to wave number topography spectra we would have $\lambda \propto T \to C_V = \lambda/T \propto \lambda^0 = \text{constant}$ ($\beta = 0$). In such a case $\gamma = \alpha$ ensuring that if $\Phi_k(k) \propto k^{-2} \to \Phi_\omega(\omega) \propto \omega^{-2}$ (same slope).
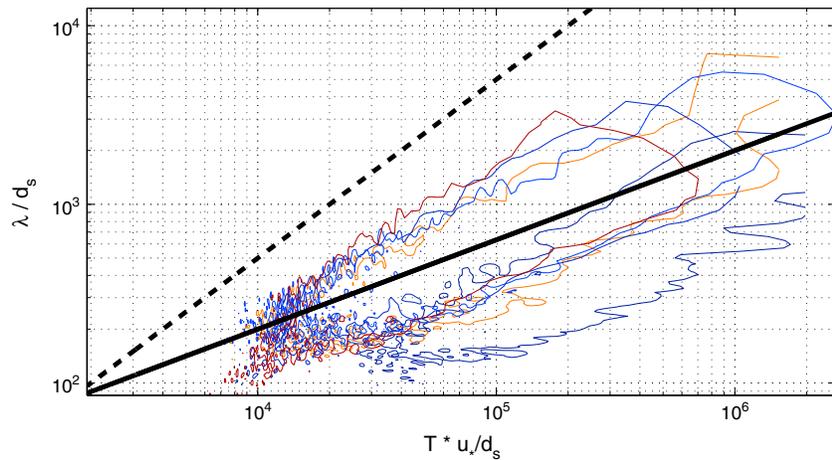
Figure 7. Dimensionless representation of the 2-D power spectra from all experiments: Note that each case is represented by a single contour line with value equal to $2 \cdot \overline{(k \cdot \omega)\Phi_{k\omega}}$ averaged in both k, ω. The solid black line of slope $1/2$ indicates the proposed power law scaling giving rise to the dimensionless form $\lambda/d_s = C(\frac{Tu_*}{d_s})^{1/2}$ with $C = 2$. The dashed line of slope 1 represents the $\lambda \propto T$ relationship valid for Taylor's hypothesis.

If Taylor's assumption is violated and the propagation velocity C_V is replaced by an expression for scale-dependent convection velocities, as, e.g., the one proposed here $C_V(\lambda) = C^2 \frac{u_* d_s}{\lambda} \propto k$ ($\beta = 1$), we obtain that a wave number spectrum $\Phi_k(k) \propto k^{-3}$ ($\alpha = 3$) is transformed into a frequency spectrum $\Phi_\omega(\omega) \propto \omega^{-2}$ ($\gamma = 2$, different slope). Note that the estimated -3 power scaling exponents in the wave number domain is in agreement with those observed and predicted by *Hino* [1968] and *Nikora et al.* [1997]. However, only one scaling regime is observed and predicted herein in the frequency domain, with a -2 exponent corresponding to the scaling regime of *Hino* [1968] (in the low-frequency range) and to the scaling regime of *Nikora et al.* [1997] (in the high-frequency range).

3.4. Generalized Expression for Scale-Dependent Convection Velocities

The ability of equation (3) to represent the 2-D contour of $(k \cdot \omega)\Phi_{k\omega}$ (Figures 6 and 7) could be explored using an exponent different from $n = 1/2$, which so far was assumed to govern the spatiotemporal conversion $\lambda = BT^n$. The resulting dimensionless expressions for scale-dependent convection velocities and spatiotemporal conversion of the topography spectra assume the general form

$$B = Cu_*^n d_s^{1-n}; \qquad \frac{\lambda}{d_s} = C\left(\frac{Tu_*}{d_s}\right)^n; \qquad C_V = B^{1/n}\lambda^{\frac{n-1}{n}} \propto k^\beta, \quad \text{with} \quad \beta = \frac{1-n}{n} \tag{6}$$

which, for the specific case $n = 1/2$, recovers equation (3). Note that the general exponent n does not modify directly the relationship $C_V \propto u_*$ between the scale-dependent convection velocity and the shear velocity. However, for each n, the value of C resulting from the fit of $(k \cdot \omega)\Phi_{k\omega}$ will change, with relevant implication for the spectral estimate of sediment transport (since $C_V \propto C^{1/n}$).

3.5. Wave Amplitude and Convection Velocity: Estimate of Sediment Transport Rate

Since each topographic scale is characterized by a specific amplitude (obtained from the 1-D spectrum) and is propagating with a specific scale-dependent velocity (obtained from the 2-D spectrum), the estimate of its (scale-dependent) contribution to sediment transport rate is possible. We propose that each surface wave, composed of moving sediment grains, gives a mass flux contribution that depends on the wave height (or amplitude) and on its propagating (or convection velocity). Hence, the total sediment transport rate can be expressed as (see Figure 1)

$$q_s = (1-p) \int_{k_{min}}^{k_{max}} A_k C_V(k) dk \tag{7}$$

where k_{min} and k_{max} are the lower and upper limits, respectively, of the scales contributing to the sediment flux (an issue we come back later to, in this section). This model can be interpreted as a scale-dependent, generalized version of *Simons et al.* [1965] model. The amplitude A_k of each spatial scale λ (or wave number k) is obtained from the 1-D power spectrum, while its convection velocity $C_V(k)$ is estimated using
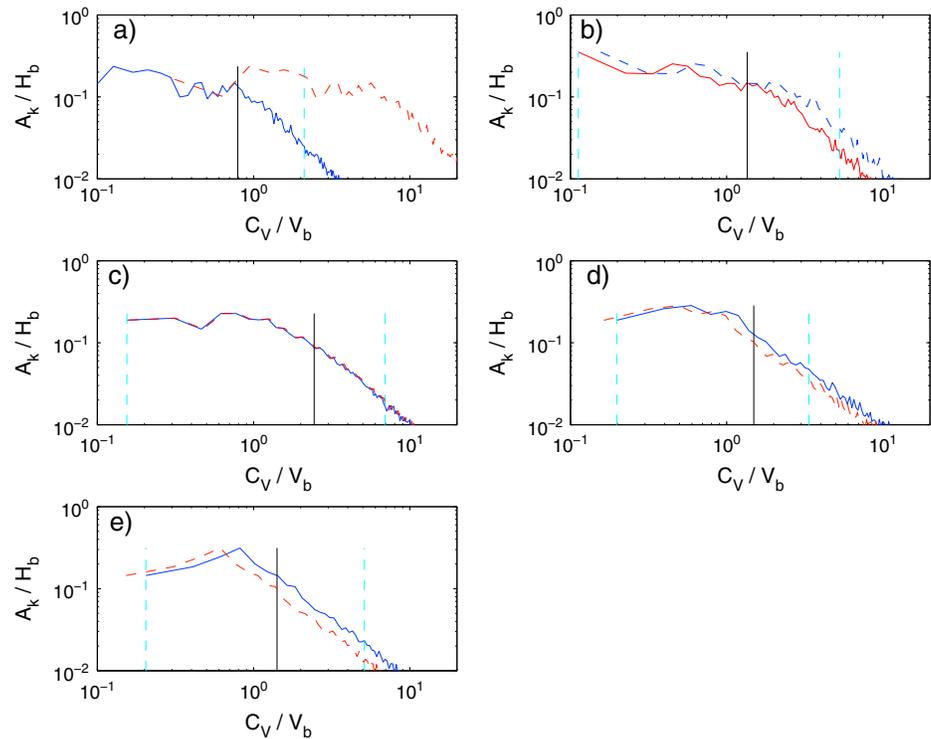
Figure 8. (a–e) Fourier amplitude A_k, normalized with the mean bed form height H_b plotted as a function of the scale-dependent convection velocities $C_v(k)$, normalized by the mean bed form velocity V_b for all cases. $C_v(K)$ is estimated using a case-specific fitted C_{var} (dashed line) and a constant $C = 2$ (solid line). Integral velocity scales are reported as vertical solid lines in each plot, while vertical dashed lines indicate the limit of integration in formula (7).

equation (6). Results, for each flow discharge and bed material composition, include the cases of constant C or variable C_{var} obtained by fitting the 2-D spectra. The relationship between A_k and $C_v(k)$ are plotted in Figure 8 for all the experiments. Note that the scaling relationships, presented in section 3.3, $\Phi_k \propto k^{-\alpha}$ and $C_v(k) \propto k^\beta$, lead to $\Phi_k \propto C_v(k)^{-\alpha/\beta} = C_v(k)^{-3}$ (for the particular case of $\alpha = 3$, $\gamma = 2$, $\beta = 1$, $n = 1/2$). Consistent with Figures 6 and 7 the proposed spatiotemporal relationship (6), for a constant value of C, does not adequately reproduce the lowest discharge experiment, leading to an overestimate of the convection velocities and, as we will observe, of the sediment transport rate.

By integrating the observed curves in the $C_v(k), A_k$ domain we obtain (i) an integral convection velocity (conceptually similar to the integral time/length scale in turbulent flows), and most importantly, (ii) the overall sediment transport contribution given by the full range of propagating scales. Because our analysis is carried out assuming homogeneity in the spanwise direction (i.e., perfectly 2-D bed forms), the contribution calculated above, in fact, is equal to the sediment discharge per unit width, usually defined as q_s [m^2 s^{-1}]. This procedure assumes that no sediment transport occurs as a wash load or in suspension. The estimated sediment transport rate results thus from only the passage of bed forms, consistent with the assumptions of *Simons et al.* [1965]. It is important to mention that the limits of integration of equation (7), k_{min} and k_{max}, were defined by the largest resolved wavelength (k_{min}), and as corresponding to a spectral amplitude $A(k) < (d_s/2)$ (k_{max}), thus neglecting the noise plateau observed in Figure 4. In theory, these limits should reflect the range of validity of the scaling relationship of equation (3). However, even in the absence of spatiotemporal information, the largest scale should comprise at least a few dominant wavelengths to make sure that bed form spatial variability can be accounted for. When more than one bed form type is observed, in equilibrium conditions, the lower limit k_{min} should be defined to include the largest migrating feature (including alternate bars, if observed). Note that in general the relative influence of the very large migrating scales included in the integration is reduced by a low-spectral amplitude $A(k)$ (expected for scales larger than the dominant wavelength) and by a low convection velocity $C_v(k)$ (always decreasing with increasing λ). Given these assumptions, the results from the proposed spectral approach are compared in Figure 9
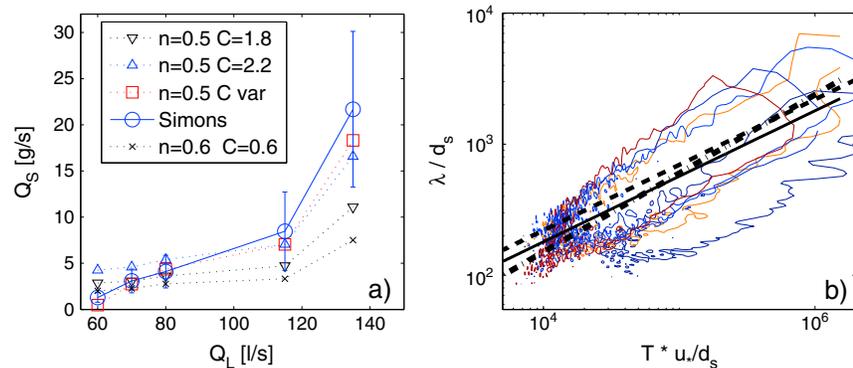
Figure 9. (a) Comparison between total sediment transport rates ($Q_s = b \cdot q_s$ where b is the channel width) obtained by *Simons et al.* [1965] method and by the proposed spectral approach (with variable C_{var} and constants $C = 1.8$ and $C = 2.2$, and different exponents $n = 0.5$–0.6); (b) the effect of varying $C = 1.8$ (solid line) and $C = 2.2$ (dashed line), while keeping $n = 0.5$, and varying exponent $n = 0.6$, $C = 0.6$ (dash-dotted line) is reflected in the different power laws representing the $(k \cdot \omega)\Phi_{k\omega}$ spectra.

to those using *Simons et al.* [1965] formula with the average bed form velocities and heights reported in Table 1.

We explore two different cases and illustrate our results in Figure 9:

1. For the sake of validating the proposed spectral method, we explore the case of variable $C = C_{var}$, obtained by fitting, for each discharge, the 2-D spectra shown in Figure 6. We first varied the exponent n between 0.45 and 0.7, obtained in each case by the best fitted B corresponding to a range of C_{var} (e.g., varying between 0.7 and 2.3 for $n = 0.5$). In such conditions, the closest agreement with *Simons et al.* [1965] results ($< 7\%$ difference) was obtained with $n = 0.47$, thus very close to the value $n = 1/2$ suggested above and included in Figure 9. This procedure proves that the spectral method provides reliable sediment transport rate estimates, once spatiotemporal measurements are available to optimize C_{var} for each discharge. This however implies that a single expression for dynamic scaling, as the one proposed as a solid line in Figure 7 is not possible.

2. For the sake of testing predictive capabilities of the spectral method, we fixed $n = 1/2$ and kept C constant for all the discharges. We found that a value $C = 2$ reasonably reproduces *Simons et al.* [1965] method estimates (with an average 25% difference), while overlapping with the $(k \cdot \omega)\Phi_{k\omega}$ spectral contour of Figure 7. For $n = 0.5$, C values in the range of 1.8–2.2 are acceptable in terms of transport rate prediction (differences $< 30\%$) and spatiotemporal spectra (Figures 9a and 9b). Note that with a slightly different exponent $n = 0.6$, we may reproduce better the trend in the spatiotemporal spectra; however, the resulting lower value of $C = 0.6$ leads to an underestimate of the sediment transport rate for all discharges.

The analysis presented above was for the purpose of exploring the predictive power of the proposed method to uncertainties in the involved parameters n and C. Since unfortunately we do not have sediment flux data for our experiments, inferences about the accuracy of our method by comparison to the results using *Simons et al.* [1965] formula must be done with caution. Several factors may contribute to the observed discrepancies between the two methods: (i) the statistical variability of bed form heights and propagation velocities ignored in Simons' formula; (ii) the subjectivity behind the bed form identification and bed form extraction characteristics procedures; (iii) the lack of phase information in the proposed spectral method; (iv) the assumption that all scale, from the grain size to the largest topographic feature, are contributing to the net transport of mass; and (v) high frequencies/wave numbers contribution resulting from the nonsinusoidal shape of migrating features. Both the spectral and *Simons et al.* [1965] sediment flux estimates were also compared with those provided by Meyer-Peter-Müller formulation [*Meyer-Peter and Müller*, 1948], a typical sediment transport formula well suited for gravel bed or coarse sand (with no bed forms), recently revisited by *Wong and Parker* [2006]. The Meyer-Peter-Müller sediment transport formula over-predicted both the bed form-based methods (spectral and Simons) by at least a factor 3 for all discharges. The major reason is that Meyer-Peter-Müller's formula was developed for flatbed conditions, implying that a relevant portion of the total drag, specifically the form drag induced by the bed form, is not contributing to transport.

It is noted that our spectral method considers only 1-D (streamwise) movement of bed forms. However, it can be extended to include explicitly lateral movement by expanding the topography $z(x, y, t)$ in the full (k_x, k_y, ω) domain, as it was done in the boundary layer case study presented by *LeHew et al.* [2011]. A full description of bed topography $z = z(x, y, t)$ may also shed some light on surface deformation processes that are not accounted for here.

4. Discussion

The presence of many topographic scales of motion in a riverbed, evidenced in Figure 7, is not accounted for in *Simons et al.* [1965] assumption of a dominant bed form type and size, migrating at a constant velocity. In this respect, a new formulation is introduced here which can incorporate the systematic deformation of different size bed forms and topographic features and translate their spatiotemporal variability into a contribution to sediment flux. The evidence for violation of Taylor's hypothesis implies that, statistically, a range of scale-dependent convection velocities is required to correctly project temporal information onto the streamwise axis, and, physically, that bed forms on average modify their shape and size while traveling downstream. This is not the result of a random deformation process acting on the amplitude, period, and size of the bed forms but rather of a systematic trend showing larger bed forms propagating slower than smaller bed forms and leaving its signature on the different slopes between spatial and temporal topography spectra (see section 3.3). This phenomenon can be attributed to bed form merging and/or to the decrease of the shear stress on top of large bed forms, causing both a spatial redistribution of the local sediment transport rate and a growth of the bed form in the cross-stream direction, with the consequence of decreasing its propagation velocity. Alternatively, in the case of coexisting bed form types, such as dunes superimposed on bars, or ripples on dunes, the smaller bed form type is the one experiencing most of the turbulent shear stresses (consistently with the Bagnold assumptions), likely sheltering the underlying larger bed form from erosional processes, and ultimately slowing down its propagation velocity.

The violation of Taylor's hypothesis suggests also that *Simons et al.* [1965] formula should not be applied using independently averaged values of bed form velocity $V_b = <V_{bf}>$ and height $H_b = <H_{bf}>$ but rather the average $<H_{bf}V_{bf}>$. In our approach we bypass the problem of explicitly estimating H_{bf} and V_{bf} for each bed form, and then averaging over their joint variability, by working directly in the 2-D frequency wave number domain (where the spatiotemporal variability is reflected in the 2-D shape, e.g., elongated versus wide, of the $\Phi_{k,\omega}$ spectra). To provide a statistical measure of the spatiotemporal bed form variability, we compare in Figure 10 the average periods $T_{bedform}$ and wavelengths $L_{bedform}$ of more than 20 bed forms (visually detected in the $z(x, t)$ domain, for each run and extracted using the *Singh et al.* [2011] method), with those resulting from the peak of the 2-D spectra, and we include vertical bars denoting the standard deviation of $L_{bedform}$ and $T_{bedform}$ for each run. Because these statistics suffer from the subjectivity of bed form classification and identification, the space-time 2-D FFT operator is inferred to be a more robust and objective estimator for topographic variability. Thanks to the λ, T dynamic scaling relationship proposed here, a simplified approach is possible using the 1-D topography spectrum, for example, from one fixed sonar measuring in time, to account for bed form size, type, and shape variability and $C_V(\lambda) = C^2 \frac{u_* d_s}{\lambda}$ to account for the bed form size-dependent propagation velocity. In summary, our method has several advantages compared to *Simons et al.* [1965] formula: (i) it accounts for the bed form spatiotemporal variability, not only for their average values, (ii) it does not need the implementation of bed form extraction techniques and the degree of subjectivity that is required to identify a bed form from bed elevation data, and (iii) using the expression for scale-dependent convection velocity, it only needs temporal or spatial time series of bed elevations with no assumptions other than the empirically derived constant $C = 2$. We infer that in natural rivers with complex topographic features, sediment transport is expected to be better described through the proposed spectral based model.

4.1. Alternative Scaling Option

Using the shear velocity u_* and the mean sediment diameter d_s in the spectra normalization and in the expression for the convection velocities has some implications for the spatiotemporal scaling of the observed bed forms. This, however, does not imply that a unique scaling regime should exist or that a model for topography spectra should be only a function of u_* and d_s. In analogy with wall turbulence, the choice of u_* and d_s as scaling quantities can be interpreted as a frictional or inner scaling normalization, emphasizing the role of the single grain as the building block of bed forms or simply as the smallest scale of topographic
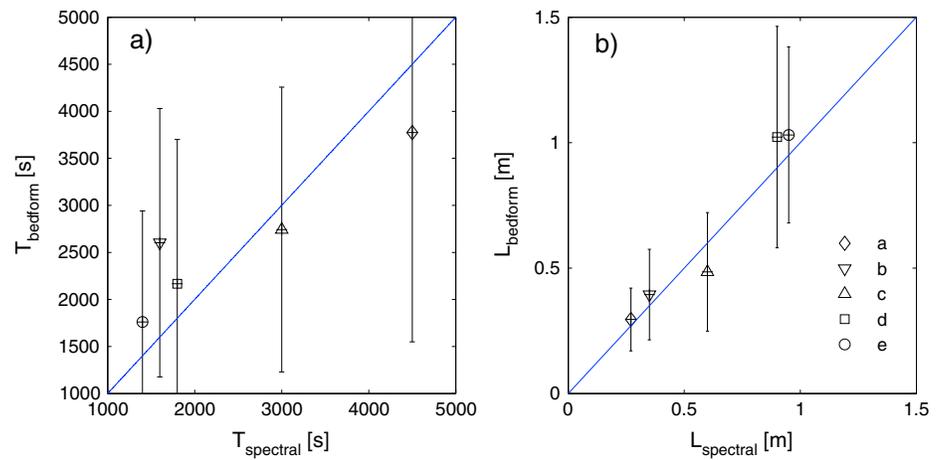
Figure 10. Comparison of the averaged (left) bed form period T and (right) bed form wavelength L with the period and wavelength corresponding to the peak in the 2-D spectra. Error bars represent 1 standard deviation, estimated over approximately 20 identified bed forms in the $z(x, y)$ domain. Experiments are marked according to Table 1.

variations. A possible alternative is provided by using an outer scale quantities such as the flow depth or the mean cross-sectional velocity. Questioning the correct normalization scale implies assessing if, at increased discharge and/or channel size, we would observe (i) a wider range of convection velocities, (ii) a change in the scaling exponent, and (iii) a change in the constant C (thus a different slope and/or offset in the solid line of Figure 7). In Figure 11 we plot the spatially and temporally averaged bed form characteristics (period and length) in the same dimensionless domain proposed in Figure 7, including additional results obtained from two experiments performed in a 3 times larger flume (data from *Singh et al.* [2011, 2012a, 2012b, SAFL Main Channel]). Figure 11 deserves a thorough interpretation:

1. When compared to the contour of the normalized 2-D spectra, bed form statistics allow for the estimate of a mean bed form propagation velocity but not of a range of scale-dependent convection velocities. Bed form variability, which partially contributes to the $\Phi_{k\omega}$ spectra is indeed lost while averaging over many identified bed forms. Therefore, from those data points, only the velocity of the statistically dominant bed form, assumed as a single length scale waveform rigidly translating, can be obtained and inferred to provide an indication of the peak of the 2-D spectra not of its shape.
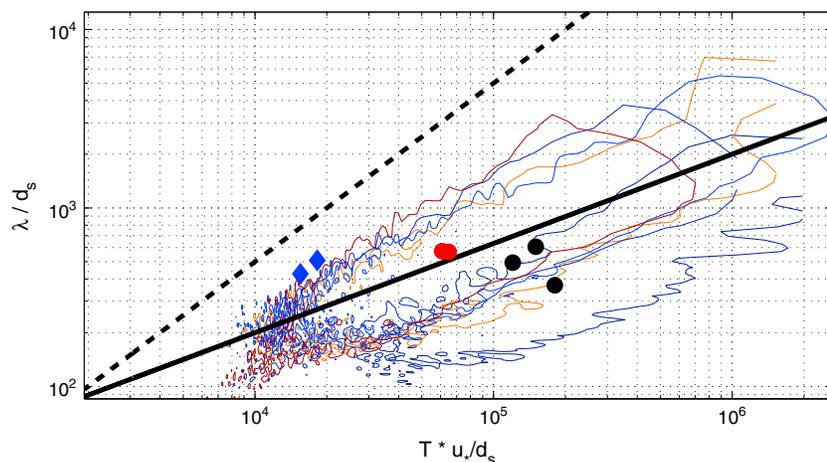
Figure 11. Selected contours from dimensionless 2-D power spectra according to inner scale normalization (see details in Figure 7). Black and red filled circles indicate the averaged bed form length L and periods T for the sand and gravel experiments, respectively. Blue diamonds indicate L, T obtained from the SAFL Main Channel experiments [*Singh et al.*, 2011, 2012a, 2012b]. The solid black line indicates the proposed power law scaling taking the dimensionless form $\lambda/d_s = C(Tu_*/d_s)^{1/2}$. The dashed line represents the $\lambda \propto T$ relationship valid for Taylor's hypothesis.

2. The larger and slower bed forms obtained in the Main Channel (with a flow depth varying from 0.44 to 0.65 m) do not seem to obey pure inner scaling as the data fall slightly outside the range of the investigated spatiotemporal spectra. A possible reason for this behavior could be the marked three dimensionality of bed forms at higher discharge and the scaling of bed forms with flow depth rather than the grain size. Without spatiotemporal data however a direct comparison between the two experiments is not possible as the evolution and deformation of the large bed forms, and thus their contribution in the Fourier decomposed λ, T domain, cannot be assessed. Dynamic scaling may still hold, in the form we proposed, but with an adjustment of the proportionality constant that may exhibit a weak dependency on u_* or the flow depth.

We acknowledge that the choice of the normalizing scaling quantities remains an open question and that the extension of the proposed dynamic scaling to rivers or large-scale channels is not straightforward. However, just estimating bed form characteristics will not solve the scaling ambiguity. Fully resolved spatiotemporal measurements are necessary to validate our method for a wider range of flow discharges and channel geometry, and especially for a wide range of bed form types. Outer scaling, replacing the sediment diameter with the mean flow depth and/or substituting the shear velocity with the mean cross-sectional velocity, is an alternative option that, at the present stage, we cannot embrace or dismiss. Future research will be devoted to extending measuring capabilities in the SAFL Main channel to obtain time-resolved topographies $z = z(x, y, t)$ allowing for a systematic study of the above questions.

5. Conclusions

A spectral description of evolving bed forms obtained in a laboratory flume under a specific range of flow discharges and with two different bed materials is provided in the temporal and spatial domain. Experiments are characterized by a variety of bed forms, typical of a laboratory scale flume, including ripples, dunes, and bed load sheets. Scale-dependent convection velocities are computed and larger structures were confirmed to propagate slower than smaller structures, thus violating the (analogue of) Taylor's hypothesis of frozen turbulence. This conclusion is reached based on a multiscale statistical analysis in the spectral domain on experimental data of bed elevation series, with no assumptions on specific bed form types or any required classification. It is further supported by a scaling functional relationship between scale-dependent wave lengths λ and periods T: specifically $\frac{\lambda}{d_s} = C \left(\frac{T u_*}{d_s} \right)^{1/2}$, where d_s is the mean sediment diameter, u_* is the shear velocity, and $C \simeq 2$ is a model parameter. We acknowledge that the above expression is consistent with the normalization of the topography spectra using the mean grain size and the shear velocity. Such a choice points at the single grain as the building block of bed forms and as the smallest scale of topographic variation. It does not imply that full similarity must be achieved across the entire spectrum, in the same way Kolmogorov scaling is not expected to satisfy the whole turbulent velocity spectrum.

The present work also leads to a generalization of *Simons et al.* [1965] approach, allowing for an estimate of sediment transport rate in the occurrence of a range of migrating surface features. Such estimate is based on a Fourier decomposition of the migrating multiscale bed topography that bypasses the problem of bed form extraction, classification, and typology-based analysis. We also explored how different power law exponents $n \neq 1/2$, and constant versus variable C, in the proposed spatiotemporal scaling $\lambda = C u_*^n d_s^{1-n} T^n$, influence the spectral estimates of sediment transport. In the range of investigated conditions, a constant C led to deviation up to 30% from Simons formula. Indications from experiments performed in a much larger facility, suggest that C may be weakly dependent on u_* or on the flow depth, opening up a whole subject for future work.

We acknowledge that the repeated longitudinal transects providing $z = z(x, t)$ do not allow us to resolve the full 3-D spectra of bed elevations (in the k_x, k_y, ω streamwise, spanwise wave numbers, and frequency domain), implying that all the observed migrating bed forms are in fact treated as spatially two dimensional, translating in the longitudinal direction only, and thus excluding 3-D deformation processes such as the amalgamation of bed forms due to lateral movement. Three-dimensional bed topography evolution under a wider range of flow discharges and bed form sizes and types, from differently scaled facilities or from field measurements, are needed to further extend the proposed formalism in the lateral direction and assess its importance in the estimation of sediment flux.

References

Aberle, J., V. Nikora, M. Henning, B. Ettmer, and B. Hentschel (2010), Statistical characterization of bed roughness due to bed forms: A field study in the Elbe River at Aken, Germany, *Water Resour. Res.*, 46, W03521, doi:10.1029/2008WR007406.

Allen, J. R. L. (1968), The nature and origin of bed-form hierarchies, *Sedimentology*, 10(3), 161–182.

Andreotti, B., P. Claudin, O. Devauchelle, O. Duran, and A. Fourriere (2012), Bedforms in a turbulent stream: Ripples, chevrons and antidunes, *J. Fluid Mech.*, 690, 94–128, doi:10.1017/jfm.2011.386.

Bagnold, R. A. (1946), Motion of waves in shallow water, interaction between waves and sand bottoms, *Proc. R. Soc. London, Ser. A*, 187, 1–15.

Best, J. (2005), The fluid dynamics of river dunes: A review and some future research directions, *J. Geophys. Res.*, 110, F04S02, doi:10.1029/2004JF000218.

Betat, A., V. Frette, and I. Rehberg (1999), Sand ripples induced by water shear flow in an annular channel, *Phys. Rev. Lett.*, 83(1), 88–91, doi:10.1103/PhysRevLett.83.88.

Chung, D., and B. J. McKeon (2010), Large-eddy simulation investigation of large-scale structures in a long channel flow, *J. Fluid Mech.*, 661, 341–364.

Coleman, S. E., and B. W. Melville (1994), Bed-form development, *J. Hydraul. Eng.*, 120, 544–560, doi:10.1061/(ASCE)0733-9429(1994)120:5(544).

Coleman, S. E., V. I. Nikora, S. R. McLean, T. M. Clunie, T. Schlicke, and B. W. Melville (2006), Equilibrium hydrodynamics concept for developing dunes, *Phys. Fluids*, 18, 105104, doi:10.1063/1.2358332.

Colombini, M., and A. Stocchino (2011), Ripple and dune formation in rivers, *J. Fluid Mech.*, 673, 121–131, doi:10.1017/S0022112011000048.

Colombini, M., G. Seminara, and M. Tubino (1987), Finite amplitude alternate bars, *J. Fluid Mech.*, 181, 213–232.

Dennis, D., and T. Nickels (2008), On the limitations of Taylor's hypothesis in constructing long structures in a turbulent boundary layer, *J. Fluid Mech.*, 614, 197–206, doi:10.1017/S0022112008003352.

Engelund, F., and J. Fredsoe (1982), Sediment ripples and dunes, *Annu. Rev. Fluid Mech.*, 14, 13–37.

Erm, L., and P. Joubert (1991), Low-Reynolds-number turbulent boundary layers, *J. Fluid Mech.*, 230, 1–44.

Fourriere, A., P. Claudin, and B. Andreotti (2010), Bedforms in a turbulent stream: Formation of ripples by primary linear instability and of dunes by nonlinear pattern coarsening, *J. Fluid Mech.*, 649, 287–328, doi:10.1017/S0022112009993466.

Jaeggi, M. (1984), Formation and effects of alternate bars, *J. Hydraul. Eng. ASCE*, 110(2), 142–156.

Paola, C., and V. R. Voller (2005), A generalized Exner equation for sediment mass balance, *J. Geophys. Res.*, 110, F04014, doi:10.1029/2004JF000274.

Giri, S., and Y. Shimizu (2006), Numerical computation of sand dune migration with free surface flow, *Water Resour. Res.*, 42, W10422, doi:10.1029/2005WR004588.

Guy, H. P., D. B. Simons, and E. V. Richardson (1966), Summary of alluvial channel data from flume experiments 1956–61, *Geol. Surv. Prof. Pap.*, 426-I, 1–96.

Hino, M. (1968), Equilibrium-range spectra of sand waves formed by flowing water, *J. Fluid Mech.*, 34(3), 565–573.

Ikeda, S. (1984), Prediction of alternate bar wavelength and height, *J. Hydraul. Eng.*, 110, 371–386.

Jerolmack, D., and D. Mohrig (2005), Interactions between bed forms: Topography, turbulence and transport, *J. Geophys. Res.*, 110, F02014, doi:10.1029/2004JF000126.

Kennedy, J. (1963), The mechanics of dunes and antidunes in erodible bed channels, *J. Fluid Mech.*, 13(2), 521–544.

Krogstad, P. A., J. H. Kaspersen, and S. Rimestad (1998), Convection velocities in a turbulent boundary layer, *Phys. Fluids*, 18, 055105, doi:10.1063/1.869617.

LeHew, J., M. Guala, and B. McKeon (2011), A study of the three-dimensional spectral energy distribution in a zero pressure gradient turbulent boundary layer, *Exp. Fluids*, 51(4), 997–1012, doi:10.1007/s00348-011-1117-z.

Martin, R., and D. Jerolmack (2013), Origin of hysteresis in bedform response to unsteady flows, *Water Resour. Res.*, 49, 1314–1333, doi:10.1002/wrcr.20093.

McElroy, B., and D. Mohrig (2009), Nature of deformation of sandy bed forms, *J. Geophys. Res.*, 114, F00A04, doi:10.1029/2008JF001220.

Meyer-Peter, E., and R. Müller (1948), Formulas for bed-load transport, *Proceedings of the 2nd Meeting of the International Association for Hydraulic Structures Research*, Stockholm, Sweden, 39–64.

Morrison, W. R. B., K. J. Bullock, and R. E. Kronauer (1971), Experimental evidence of waves in the sublayer, *J. Fluid Mech.*, 47, 639–656.

Nikora, V. I., A. N. Sukhodolov, and P. M. Rowinski (1997), Statistical sand wave dynamics in one-directional water flows, *J. Fluid Mech.*, 351, 17–39.

Nordin, C. F., and J. H. Algert (1966), Spectral analysis of sand waves, *J. Hydraul. Div. Am. Soc. Civ. Eng.*, 92(HY5), 95–114.

Rubin, D. M., and D. S. McCulloch (1968), Single and superimposed bedforms: A synthesis of San Francisco Bay and flume observations, *Sediment. Geol.*, 26(1-3), 207–231, doi:10.1016/0037-0738(80)90012-3.

Schwämmle, V., and H. J. Herrmann (2004), Modelling transverse dunes, *Earth Surf. Process. Landforms*, 29(6), 769–784.

Seminara, G. (2010), Fluvial sedimentary patterns, *Annu. Rev. Fluid Mech.*, 42, 43–66, doi:10.1146/annurev-fluid-121108-145612.

Simons, D. B., E. V. Richardson, and C. F. Nordin Jr (1965), Bedload equation for ripples and dunes, *U.S. Geol. Surv. Prof. Pap.*, 462(H), 1–9.

Singh, A., S. Lanzoni, P. R. Wilcock, and E. Foufoula-Georgiou (2011), Multi-scale statistical characterization of migrating bedforms in gravel and sand bed rivers, *Water Resour. Res.*, 47, W12526, doi:10.1029/2010WR010122.

Singh, A., M. Guala, S. Lanzoni, and E. Foufoula-Georgiou (2012a), Bedform effect on the reorganization of surface and subsurface grain size distribution in gravel bedded channels, *Acta Geophys.*, 60-6, 1607–1638, doi:10.2478/s11600-012-0075-z.

Singh, A., E. Foufoula-Georgiou, F. Porté-Agel, and P. R. Wilcock (2012b), Coupled dynamics of the co-evolution of bed topography, flow turbulence and sediment transport in an experimental flume, *J. Geophys. Res.*, 117, F04016, doi:10.1029/2011JF002323.

Stegner, A., and J. Wesfreid (1999), Dynamical evolution of sand ripples under water, *Phys. Rev. E*, 60(4), 3487–3490.

van der Mark, C. F., A. Blom, and S. J. M. H. Hulscher (2008), Quantification of variability in bedform geometry, *J. Geophys. Res.*, 113, F03020, doi:10.1029/2007JF000940.

Venditti, J., M. Church, and S. Bennett (2005a), Bed form initiation from a flat sand bed, *J. Geophys. Res.*, 110, F01009, doi:10.1029/2004JF000149.

Venditti, J., M. Church, and S. Bennett (2005b), Morphodynamics of small-scale superimposed sandwaves over migrating dune bedforms, *Water Resour. Res.*, 41, W10423, doi:10.1029/2004WR003461.

Wong, M., and G. Parker (2006), Reanalysis and correction of bed-load relation of Meyer-Peter and Müller using their own database, *J. Hydraul. Eng. ASCE*, 132, 1159–1168.